MACHINE LEARNING TECHNIQUES FOR LAND USE/LAND COVER CLASSIFICATION OF MEDIUM RESOLUTION OPTICAL SATELLITE IMAGERY FOCUSING ON TEMPORARY INUNDATED AREAS

Boudewijn van Leeuwen*, Zalán Tobak, Ferenc Kovács

Department of Physical Geography and Geoinformatics, University of Szeged, Egyetem u. 2-6, 6722 Szeged, Hungary
*Corresponding author, e-mail: Corresponding author: leeuwen@geo.u-szeged.hu

Abstract

Classification of multispectral optical satellite data using machine learning techniques to derive land use/land cover thematic data is important for many applications. Comparing the latest algorithms, our research aims to determine the best option to classify land use/land cover with special focus on temporary inundated land in a flat area in the south of Hungary. These inundations disrupt agricultural practices and can cause large financial loss. Sentinel 2 data with a high temporal and medium spatial resolution is classified using open source implementations of a random forest, support vector machine and an artificial neural network. Each classification model is applied to the same data set and the results are compared qualitatively and quantitatively. The accuracy of the results is high for all methods and does not show large overall differences. A quantitative spatial comparison demonstrates that the neural network gives the best results, but that all models are strongly influenced by atmospheric disturbances in the image.

Keywords: Sentinel 2, artificial neural network, random forest, support vector machine, machine learning, classification

INTRODUCTION

Accurate data about land use/land cover (LULC) of our surroundings continues to be important information for many applications like the monitoring and management of natural resources, development strategies, and global change studies. LULC changes due to changes in for example biological diversity, climate and terrestrial ecosystems, but are also drivers of change for these systems (Baamonde et al., 2019; Chatziantoniou et al., 2017). Satellite data classification for mapping of LULC is a common approach. Automatic classification of LULC with high accuracy based on medium resolution optical satellite imagery has been a challenge for decades. In earlier days, spatial and temporal resolution of the input data were limiting factors for accurate monitoring of LULC change. With the appearance of global medium to high resolution multispectral satellite data with a temporal resolution of just several days, in many situations input data for LULC change studies is available in abundance, even in situations where the phenomena change quickly. Advanced algorithms to process and classify large amounts of data can be used to produce accurate thematic maps over large areas and in a timely manner.

Supervised algorithms are a common approach to extract thematic information from multispectral satellite images. This research applied different nonparametric, machine learning algorithms for classification, namely support vector machine (SVM), random forest (RF) and deep artificial neural network (ANN).

Random Forest has been developed rapidly and has been widely used in many fields such as medicine, economics, and geography during the past twenty years. Breiman (2001) proposed Random Forest, which changes the way the classification or regression tree is constructed. It is an ensemble classification method consisting of many decision tree classification models (Jin et al., 2018). The RF algorithm exhibits good robustness compared to other traditional methods in the classification of a remote sensing image, because it requires fewer parameters, minimal manual intervention, and yields high classification accuracy; it can also manage high-dimensional data and obtain classification results rapidly (Ming et al., 2016). SVM employs optimization algorithms to locate the optimal boundaries between classes. Statistically, the optimal boundaries (hyperplanes) should be generalized to unseen samples with least errors among all possible boundaries separating the classes, therefore minimizing the confusion between classes (Huang et al. 2002). SVM were originally designed as a binary linear classifier, which assumes two linearly separable classes to be partitioned. SVM are further extended to deal with non-linear classification by using a non-linear kernel function to replace the inner product of optimal hyperplane. Moreover, SVM have been used for multi-class mapping through reducing the multi-class problem into a set of binary problems so that the basic SVM principles can be still applied (Shi and Yang, 2015). SVM and RF are able to deal with unbalanced data. Therefore, SVM and RF are becoming increasingly popular in image classification studies (Thanh and Kappas, 2018; Gudmann et al., 2019). In the 2000-s, (deep) neural networks started to make their

comeback due to the increased availability of data, optimization of the training algorithms and network architectures, and improvements of hardware, mainly the availability of affordable GPUs (Zhu et al., 2017). Recently, this development was combined with easier access to the algorithms via open source machine learning libraries, like scikit-learn, Pytorch and Keras-Tensorflow (Pedregosa et al., 2011; Paszke et al., 2019; Chollet, 2015; Abadi et al., 2015). Using open source programming language Python, these libraries can be used in combination with scientific data processing libraries like pandas, numpy, matplotlib and gdal.

This research aims to classify LULC based on a Sentinel 2 satellite image with special focus on inland excess water (IEW). This is a type of inundation that occurs in regions with very low relief intensity, where large areas get flooded due to a combination of a surplus of water, and limited infiltration and evaporation, or due to upwelling of groundwater. Due to its geographical characteristics the Great Hungarian Plain is particularly vulnerable to this phenomenon. IEW mostly occurs in agricultural areas where it results in reduced production and financial loss. Long term inundations cause reduced quality of agricultural soil (Szatmári and Van Leeuwen, 2013). Quite some earlier research has been published using traditional and more novel algorithms to extract inland excess water inundations from satellite data. Maximum likelihood classification was applied to identify IEW by Rakonczai et al. (2001) and Van Leeuwen and Tobak (2014). Szántó et al. (2008) applied unsupervised classification with a self-organising map to identify IEW. Mucsi and Henits (2010) applied spectral mixture analysis in a subset of our research area but with different classes. Van Leeuwen et al. (2012) applied a small feed forward multilayer perceptron to detect inland excess water on a mosaic of aerial photographs, spectral angle mapping was applied to hyperspectral data by Csendes and Mucsi (2017), Balázs et al (2018) used Random forest and SVM and received overall accuracies of over 90% while classifying PCA data extracted from Landsat 7 data. Other methods to extract water from medium resolution satellite data have been based on various indices (Lacaux et al., 2007; Feyisa et al., 2014). Szantoi et al. (2015) presents a comparison between maximum likelihood, decision tree and feed forward multilayer perceptron algorithms to classify different types of grass in a wetland area. Our research compares the results of SVM, RF and a deep ANN to detect LULC classes with inland excess water represented by two water classes. The accuracy of the results is statistically compared using overall accuracy and Cohen's Kappa.

DATA AND STUDY AREA

The research is focused on an area in the south of the Great Hungarian Plain that is vulnerable to inland excess water (Fig. 1). On average IEW inundations occur every two to three years in Hungary. The latest IEW period was in 2018, with moderate inundations in February and March. A Sentinel 2B Level 2A image (Drusch et al., 2012) from 18 March 2018 has been selected to test the different algorithms. Sentinel 2 L2A images contain Bottom Of Atmosphere (BOA) reflectance values stored in 100 x 100 km tiles. Bands
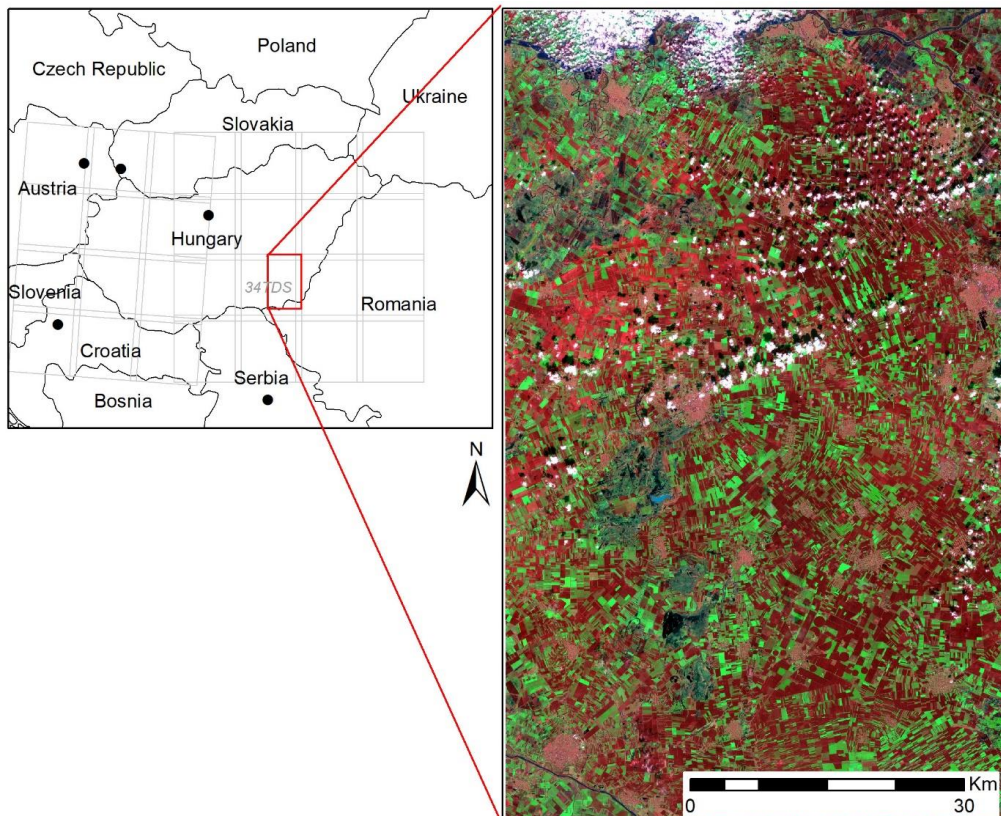

Fig. 1 Sentinel 2 false color composite (RGB843) showing the study area, its location in Hungary and the 34TDS tile in the Sentinel 2 tiling grid

2-8, 11 and 12 with spatial resolutions of 10 and 20 meter have been resampled to 10 meter and stacked into one composite file with 9 bands. Part of the original 34TDS tile did not have reflectance information due to the diagonal orientation of the satellite path compared to the Sentinel 2 tiling grid and was therefore cut off not to disturb the classifications. To exclude artifacts due to mosaicking, only one Sentinel 2 tile was used for the classifications, this way an area of 4900 km^2 remained to be classified. As usual during IEW periods, the image showed clouds and cloud shadows, which have a strong disturbing influence on classifications. The land use in the area is mainly agricultural, but there are several smaller cities and towns. In the north, the area is bounded by the Körös river, in the center and northwest larger natural wetlands and grasslands can be found (Mezősi, 2017). With elevations between 77 m and 105 m (above Baltic mean sea level) the relief intensity in the area is very small.

METHODS

Each experiment to classify the satellite image was designed in the same way (Fig. 2). First, the sample data was split into the three sets. Then, the inputs of the training and validation sets were standardized. In the next step, a model was defined as described in the next session. Several hyperparameters were tested for each model and once the optimal hyperparameters were determined, the model was trained using these hyperparameters. Then, the complete satellite image was imported and converted to a large 9-dimensional numpy array. The arrays were split into smaller subarrays to reduce memory use. The subarrays were sequentially fed to the trained model to predict new outputs. These outputs were concatenated to form an array with the same number of rows and columns as the input satellite image. The output array was then converted to a geoTiff file to be evaluated in a geographic information system (GIS). In the GIS, the test points were used to extract the classes from the model output (prediction) and compared to the actual classes (reference). Finally, a confusion matrix, overall accuracy and Cohen's Kappa were calculated.

Creation of the training, validation and test data set

Supervised classification methods require a large set of samples of input and output data to train the model to recognize the patterns forming the classes in the data set. A second data set is needed to define the hyperparameters and to validate if the model is not overfitting during the training phase. A third data set is used to independently test the predictions made using the trained model. To create the three datasets, polygons were digitized, by visual inspection of the different land cover classes on different RGB composites of the Sentinel 2 image. For each polygon, it was stored which class it represented. Then, the polygons were randomly split into three categories according to a 60/20/20 ratio and finally, they were converted to points (Fig. 3). Each point is a sample from one of eight LULC classes (Table 1).
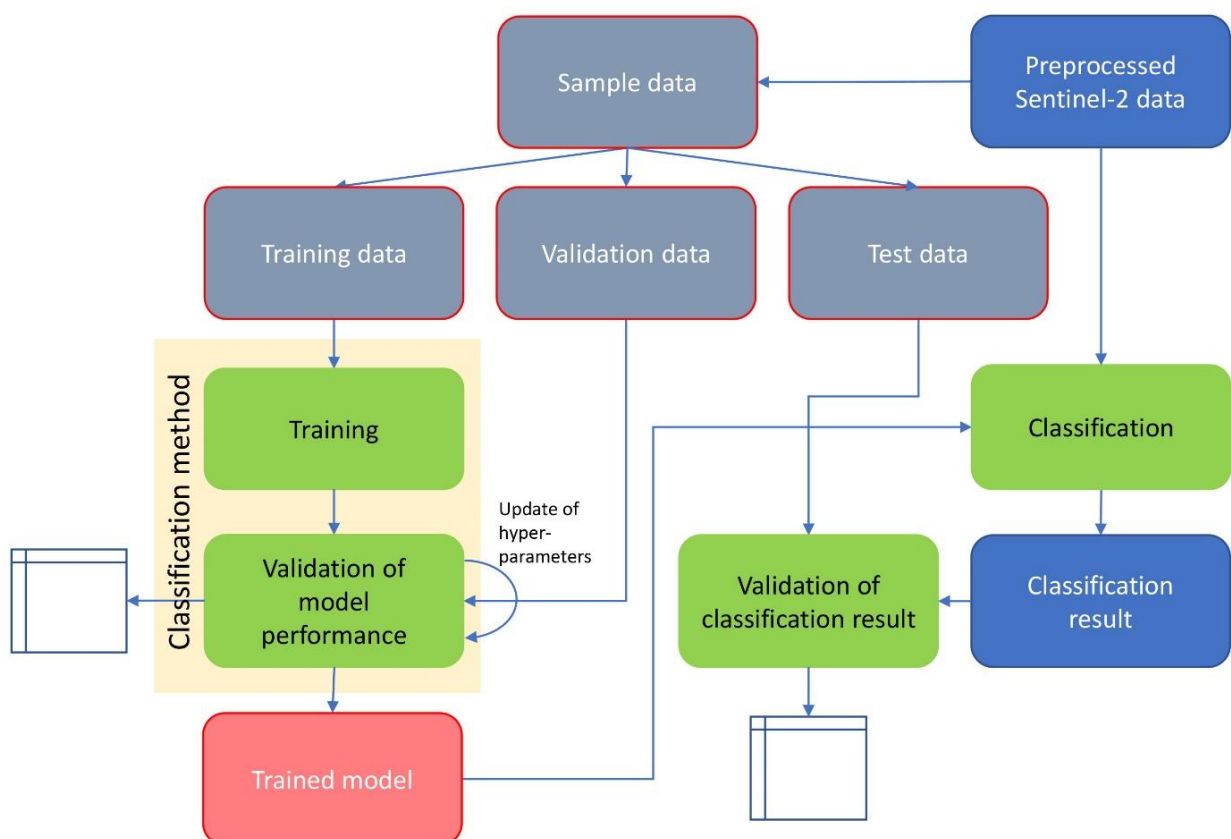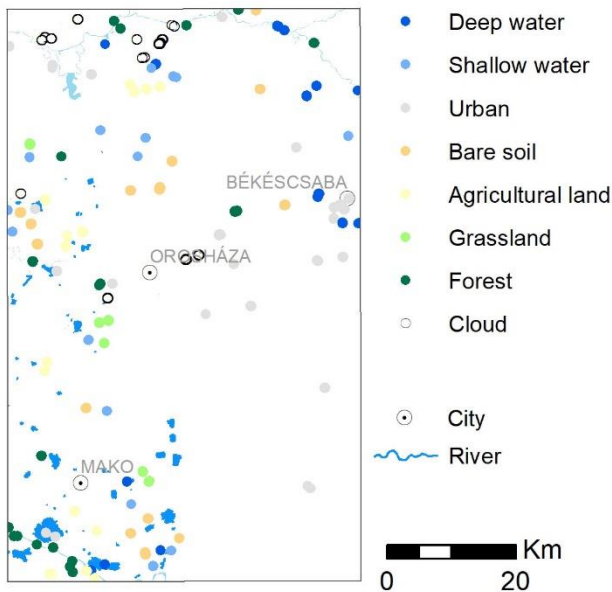

Fig. 2 Classification methodology

Fig. 3 Distribution of test points for each class in the study area

Table 1 Number of samples per LULC class in the training, validation and test sets

	LULC class	Number of samples		
		Training	Validation	Test
1	Deep water	1825	1040	1068
2	Shallow water	846	694	292
3	Urban	5294	2358	3112
4	Bare soil	6095	2733	2973
5	Agricultural land	2958	1597	1881
6	Grassland	1475	681	847
7	Forest	2805	2157	1668
8	Cloud	3793	2127	1585
	Total	25091	13387	13426

For each of the modelling algorithms, the same training, validation and test set was used. Each set was standardized by removing the mean and scaling to unit variance using Standard Scaler from the Scikit-learn library (Pedregosa et al., 2011).

Modelling

Three different models have been used to determine the best classification result. With the Scikit-learn gridSearch function many different hyperparameter combinations were evaluated and only results calculated using the optimal combinations are presented here. The first classification model is the Random Forest method. It was determined that the best result was reached with 200 trees in the forest and a maximum depth of 20 trees. The second method is the Support Vector Machines algorithm. For the kernel, a linear and an RBF kernel were tested, and the linear kernel showed better results. The regularization parameter C was set to 1.0.

The final model was a sequential deep artificial neural network with two hidden layers with 16 and 12 neurons in each layer built with Keras/Tensorflow (Abadi et al., 2015). This neural network is considered a deep neural network since it has two hidden layers, contrary to shallow neural networks with maximum one hidden layer. After each hidden layer, 20% dropout occurred to prevent overfitting. ReLu activation functions were used for the hidden layers and a softmax function for the output layer. The Adam optimization function with a learning rate of 0.001 was used for training. The ANN was trained with a batch size of 32 and 50 epochs on a Graphical processing unit (GPU). While training the model, 10-fold cross validation was calculated to determine the mean accuracy and variance (Chollet, 2015).

Prediction on the complete image using the trained model

After each model was trained, it was fed with the complete satellite image. Since the image dimension is 7382 x 8921 x 9 (columns x rows x bands) with 32 bits values, it was too large to fit it as a whole to the model. Therefore, after converting the image to a 3-dimensional numpy array, it was split in equal subarrays with a dimension of more or less 1000 x 1000 x 9. Each of the subarrays was then fed to the models and the prediction was calculated. The resulting predictions were concatenated to the original shape of the input numpy array and then the reconstructed array was exported to a TIFF image with the same spatial extent and coordinate system as the input satellite image.

Testing

The classified output image was read into a geographic information system (GIS) and at the locations of the random test points the classes were extracted. These classes were evaluated with the user defined classes at the same locations. Finally, a confusion matrix with overall accuracy and Cohen's Kappa were calculated to determine the independent validation accuracy (Congalton and Green, 2008).

RESULTS AND DISCUSSION

Qualitative assessment of the training and validation samples

The results of the predictions have been compared in a qualitative as well as quantitative matter. The qualitative comparison was performed on the whole image and on smaller areas with interesting features. To understand the distribution of the training and validation data sets, the distributions of the different classes were compared per satellite band (Fig. 4). The cloud class is not shown because in each band it is well separated from the other classes with much higher reflectance values. The training and validation samples have been randomly selected from all samples, which is reflected by the similarities of the patterns shown in both graphs. It can also be seen that the variation between the deep and shallow water classes is large, compared to urban, bare soil and grass land among most bands. Agricultural soil has the largest variation in band 6, 7 and 8. Forest has the largest variation in the bands with the longest wavelengths. Furthermore, it shows
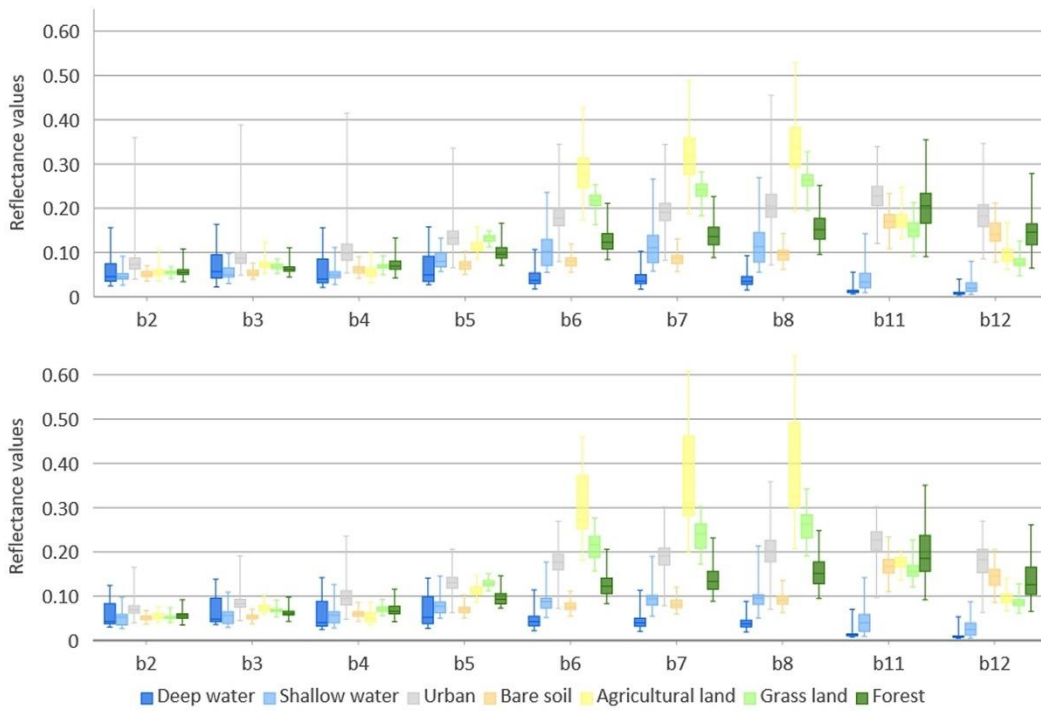
Fig. 4 Distribution of reflectance values for each class per band of the Sentinel 2 image for the training (top) and the validation set (bottom)
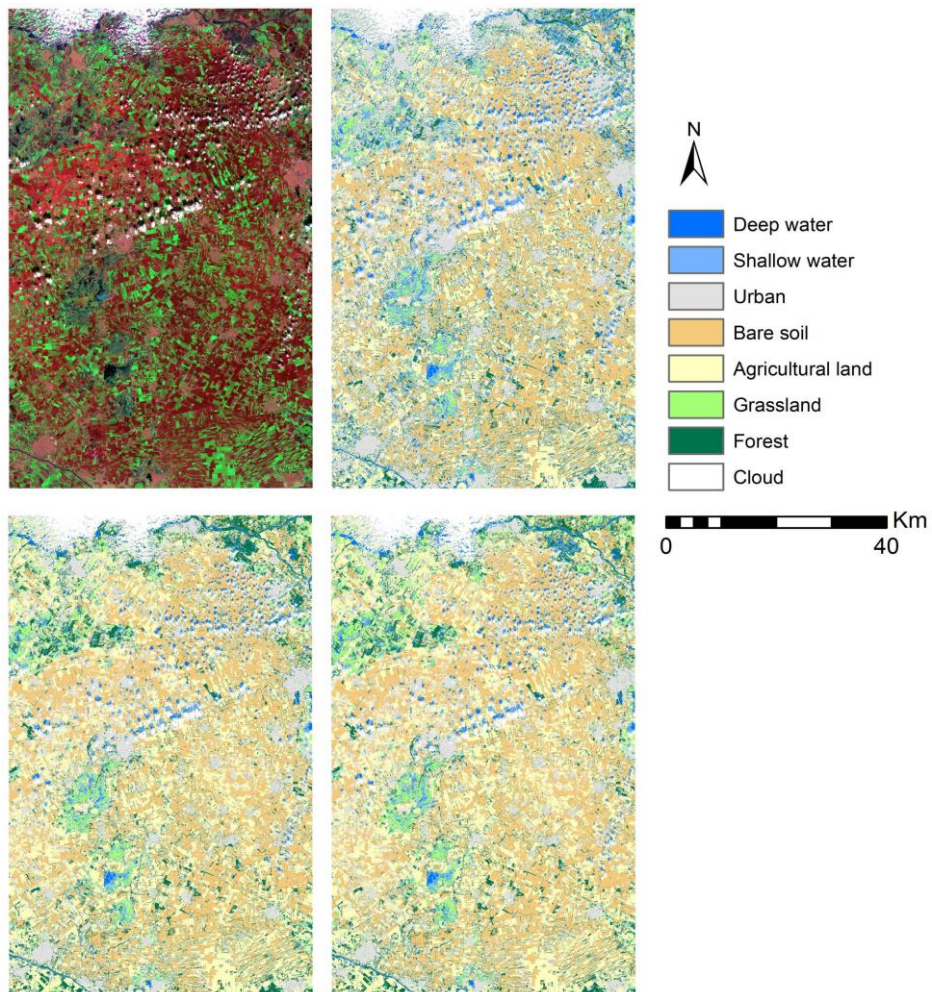

Fig. 5 Classification results for the total area: Sentinel 2 false color composite (RGB843) (upper left), Random forest result (upper right), SVM result (lower left), ANN result (lower right)

that, as expected, the variance between the reflectance values is the lowest in the bands with the shortest, visible wavelengths.

Qualitative comparison of the classification results

Visual inspection of the classification results shows a very similar pattern for all classification methods (Fig. 5). Large areas with continuous clouds in the north and scattered clouds in the center and top part of the images can be recognized in each result. Also, the pattern of large water bodies and urban centers in the area is shown in all three result. The mixture of bare soil and agriculture, typical for March in this area, is dominating the overall LULC pattern in the classifications. Overall, the classification results for SVM and ANN are more similar than for Random forest. This is confirmed by the total number of pixels classified in each class per method (Fig. 6).

Evaluating a smaller area with a large lake, surrounded by a mixture of wetland and grassland clearly shows differences between the Random forest, Support vector machine and Artificial neural network approaches (Fig. 7). The large, shallow lake in the south part of the subset is misclassified as urban by the RF method, SVM partly identifies the lake, while it is properly delineated by the ANN approach. All approaches overestimate the amount of urban in the area, but RF does this more often than the other approaches. Also, in many places, RF identified grassland is as scattered water pixels. The classification of bare soil and agricultural land is similar.

A subarea with more forests is shown in Figure 8. The forests along the river in the center are properly delineated by all approaches, but there are large differences between the amount of water south of the river where large parcels with soil heavily saturated with water can be found. ANN and RF classify these parcels almost exclusively as shallow water, while SVM designated them as forests. Many areas are misclassified as urban in the RF classification.

The third subarea is showing an urban area surrounded by a mixture of agricultural land and bare soils (Fig. 9). The urban area is classified similarly in all three approaches, but the small river and its banks flowing through the small city is only shown in the RF result. In SVM and ANN only the forest on the riverbanks is detected. Overall, the RF method is more sensitive to water than the other methods.
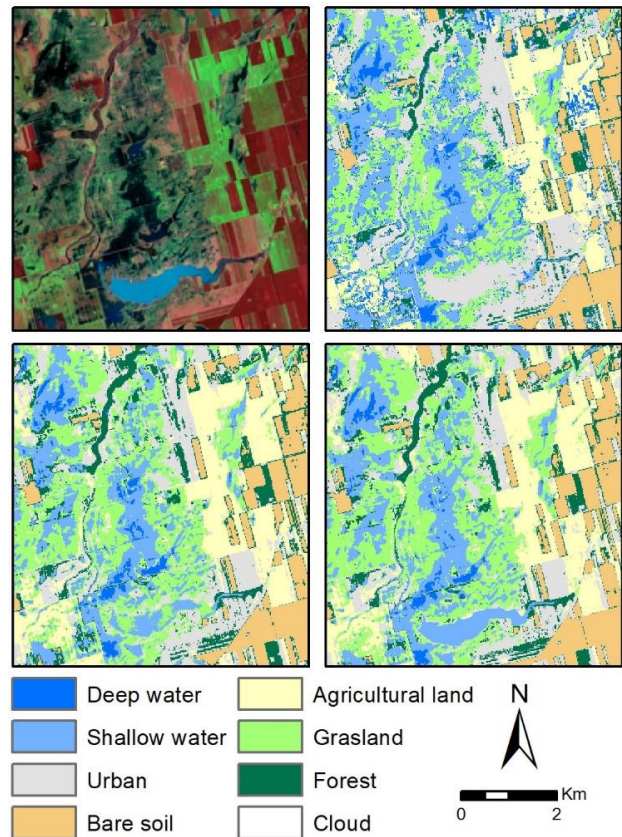

Fig. 7 Subset of the classification results with mainly inland excess water, wetlands and agriculture: Sentinel 2 false color composite (RGB843) (upper left), Random forest result (upper right), SVM result (lower left), ANN result (lower right)
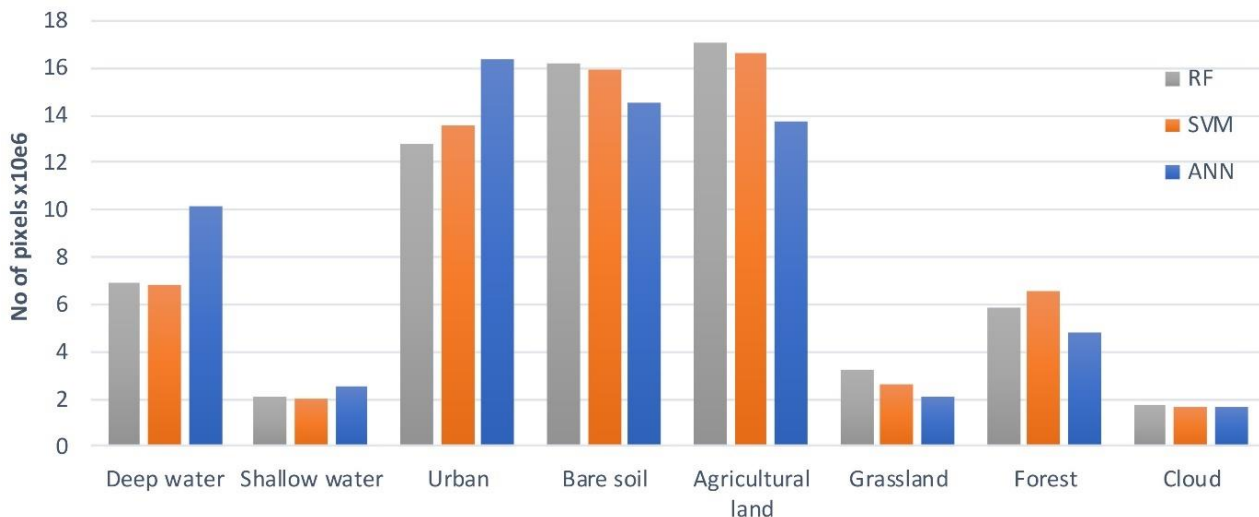

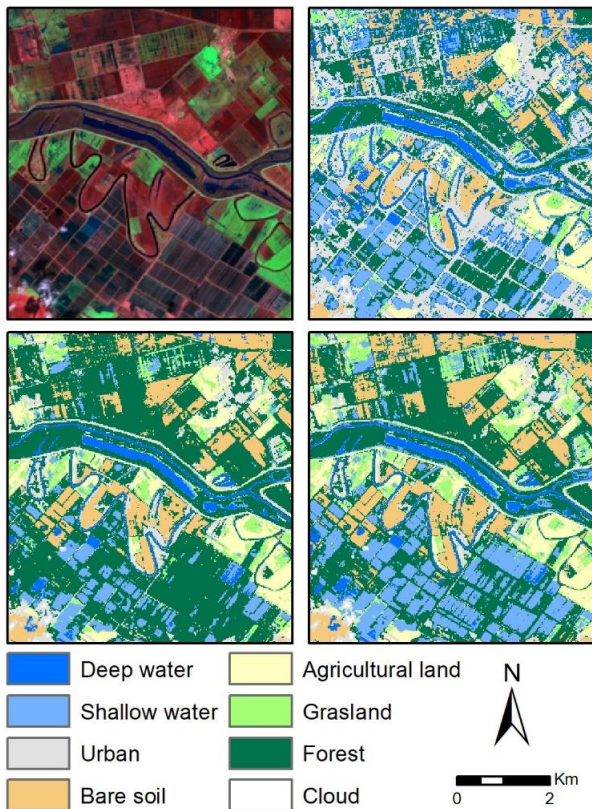*Fig. 6* Number of pixels per class for each classification method

Fig. 8 Subset of the classification results with a mixture of open water, inland excess water and saturated soils: Sentinel 2 false color composite (RGB843) (upper left), Random forest result (upper right), SVM result (lower left), ANN result (lower right).

Fig. 9 Subset of the classification results with mainly urban land use and agricultural land and bare soil: Sentinel 2 false color composite (RGB843) (upper left), Random forest result (upper right), SVM result (lower left), ANN result (lower right).
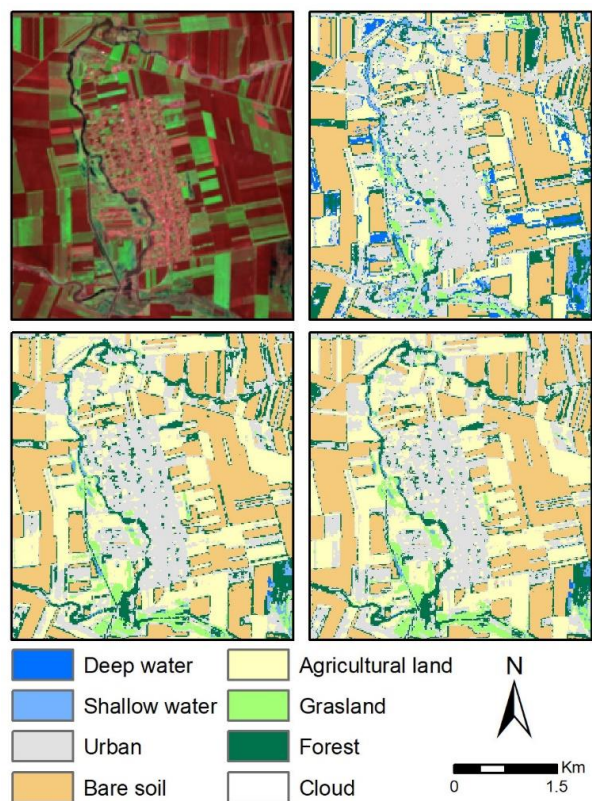
The last subarea shows the effect of clouds and cloud shadows on the classifications (Fig. 10). In all three methods, this causes problems, even though a cloud class was added to the training set. The clouds themselves are classified properly, although at their boundaries, where they are less thick, they cause every method to misclassify them as urban. The cloud shadows cause bigger problems. Without exception, the shadows are misclassified as deep or shallow water due to their darkening effect on the land cover. Often bare soil is misclassified as deep water, while agricultural land is wrongly identified as shallow water.
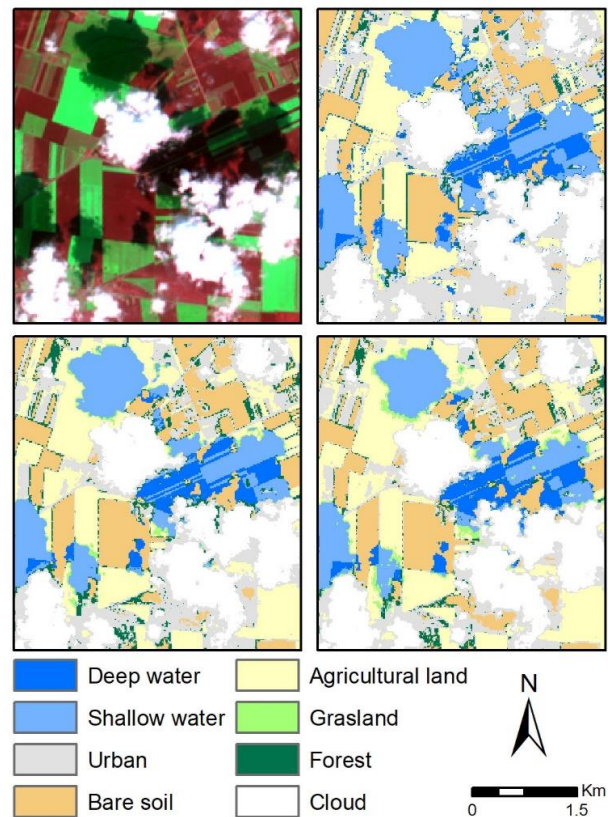

Fig. 10 Subset of the classification results with clouds and cloud shadows: Sentinel 2 false color composite (RGB843) (upper left), Random forest result (upper right), SVM result (lower left), ANN result (lower right)

Quantitative comparison of the classification results

Apart from the visual comparison between the classification results, two quantitative comparisons have been performed to evaluate the methods. The first comparison provides the average accuracy and its variation for each method based on a 10-fold cross validation calculated using the validation set. The second method is based on the test set that was used to calculate the confusion matrix giving the results from the trained models and the expected results. Based on the confusion matrix, the overall accuracy (OA), User's accuracy, producer's accuracy and Cohen's Kappa were calculated (Congalton and Green, 2008).

The Random Forest method had an average accuracy on the cross validation of 0.9275, with a variation of 0.0381. The confusion matrix is shown in Table 2. The urban prediction class contained most misclassified pixels, mainly agricultural land, grassland and forest. To

a smaller extent, these classes were also classified as deep water. The bare soil, grassland and clouds output classes never contain wrongly classified pixels.

Compared to RF, the support vector machine approach has a higher average accuracy of 0.9724 with a lower variation of 0.0184, while the test results with the independent data set are also slightly better (Table 3). Most misclassification occurred in the urban class. These are mainly agricultural land and grassland, and to a lesser extent forest and clouds. Also urban was misclassified as forest and grassland as agricultural land.

Finally, the ANN has a slightly lower average accuracy of 0.9628 with a variation of 0.0258. The test results with the independent data set is very similar (Table 4). The misclassification pattern for ANN is more or less the same as for the SVM method, although some forest was also misclassified as shallow water.

All three methods gain very high accuracy classification results (above 0.9), with RF having the lowest accuracies and SVM having very similar, but slightly better results than ANN. Comparing the training times for the three algorithms, it is clear that training the SVM model (0.567 seconds) is much more efficient than the other models (RF: 18.8 seconds, ANN: 157 seconds).

Although, in general water can usually be detected with high accuracy in multispectral images, in case of the ANN model there was a relatively high error due to misclassification as forest. This might be caused by the forests in shallow water along the Tisza river in the study area. RF and SVM did not show this misclassification. Deep water was classified almost perfectly by SVM and ANN, but RF had more problems with this class, with misclassifications in multiple other classes. All three classifications show relatively large errors for the urban class. The main reason for this might be the mixed pixels in the urban class due to the resolution of Sentinel 2 data. Agricultural land and grassland are mixed by the SVM and

ANN classifications which can be explained by thematic misclassification of the training samples.

Misclassifications often happened in areas with shadow from clouds. To overcome this problem, many methods have been developed, ranging from shadow modelling, cloud and shadow masking, to sampling of classes in the shadows (Shahtahmassebi et al., 2013; Foga et al., 2017). The aim of this research was to evaluate the differences between the selected algorithms therefore the cloud/shadow problem has been ignored in the calculations.

The data sets that have been used for training the models is relatively small. In the current revolution of deep learning the larger the data set, the better for deep neural networks. A larger training set may therefore result in higher accuracy for the ANN, but of course this will also result in longer training times. For the current classifications, the accuracy is already well above 0.90, therefore the need for higher accuracy is not apparent for the presented LULC application with relatively few classes. If the number of classes would increase, more training is required and the advantage for ANN would be higher (Rai et al., 2020).

Experiments were executed to automatically extract LULC classes from the Corine Land Cover 2018 database (CLC 2018) and use these as labels for the training data sets. Unfortunately, this method to automatically create a larger training data set was not successful because the spatial and thematic resolution of CLC2018 compared to Sentinel 2 data is too low resulting in many mixed classes within one CLC2018 polygon. Training the models with these labels caused large errors. The application of other land cover data sets with higher resolution, like Copernicus High Resolutions layer (Büttner, 2012) or National Ecosystem Base map (Tanács et al., 2019) may provide better results.

The classification algorithms were applied to data from the Sentinel 2 satellite, but can be applied to any medium resolution multispectral satellite data set.

Table 2 Confusion matrix with the random forest predictions in the columns and the true values (test set) in the rows

RF	Deep water	Shallow water	Urban	Bare soil	Agricul-tural land	Grassland	Forest	Cloud	Total	Users acc
Deep water	1067	1	0	0	0	0	0	0	1068	0.9991
Shallow water	0	291	1	0	0	0	0	0	292	0.9966
Urban	8	0	3045	0	15	0	44	0	3112	0.9785
Bare soil	2	0	0	2971	0	0	0	0	2973	0.9993
Agricultural land	32	0	160	0	1689	0	0	0	1881	0.8979
Grassland	37	0	157	0	29	624	0	0	847	0.7367
Forest	44	0	251	0	0	0	1373	0	1668	0.8231
Cloud	0	0	3	0	0	0	0	1582	1585	0.9981
Total	1190	292	3617	2971	1733	624	1417	1582	13426	
Prod acc.	0.8966	0.9966	0.8419	1.0000	0.9746	1.0000	0.9689	1.0000		

OA	0.9416
Kappa	0.9299

Table 3 Confusion matrix with the Support Vector Machine predictions in the columns and the true values (test set) in the rows

SVM	Deep water	Shallow water	Urban	Bare soil	Agricul-tural land	Grassland	Forest	Cloud	Total	Users acc
Deep water	1066	1	0	0	0	0	1	0	1068	0.9981
Shallow water	0	289	1	0	0	1	1	0	292	0.9897
Urban	0	0	3000	0	29	0	83	0	3112	0.9640
Bare soil	0	0	0	2973	0	0	0	0	2973	1.0000
Agricultural land	0	0	130	0	1751	0	0	0	1881	0.9309
Grassland	0	0	71	0	103	673	0	0	847	0.7946
Forest	0	0	21	0	0	1	1646	0	1668	0.9868
Cloud	0	0	16	0	0	0	0	1569	1585	0.9899
Total	1066	290	3239	2973	1883	675	1731	1569	13426	
Prod acc.	1.0000	0.9966	0.9262	1.0000	0.9299	0.9970	0.9509	1.0000		

OA	0.9658
Kappa	0.9591

Table 4 Confusion matrix with the artificial neural network predictions in the columns and the true values (test set) in the rows

ANN	Deep water	Shallow water	Urban	Bare soil	Agricul-tural land	Grassland	Forest	Cloud	Total	Users acc
Deep water	1065	3	0	0	0	0	0	0	1068	0.9972
Shallow water	0	291	1	0	0	0	0	0	292	0.9966
Urban	0	0	2953	3	69	0	87	0	3112	0.9489
Bare soil	0	0	0	2973	0	0	0	0	2973	1.0000
Agricultural land	0	0	110	0	1771	0	0	0	1881	0.9415
Grassland	0	6	45	0	121	675	0	0	847	0.7969
Forest	2	37	28	0	0	0	1601	0	1668	0.9598
Cloud	0	0	3	0	0	0	0	1582	1585	0.9981
Total	1067	337	3140	2976	1961	675	1688	1582	13426	
Prod acc.	0.9981	0.8635	0.9404	0.9990	0.9031	1.0000	0.9485	1.0000		

OA	0.9616
Kappa	0.9542

CONCLUSION

Automatic supervised classification of multispectral satellite imagery is required to extract land use / land cover data for a wide range of applications. Machine learning algorithms are the most promising techniques to reach this goal. The field is developing rapidly, and new algorithms and implementations are becoming available continuously. The application of machine learning algorithms in LULC classification can result in high quality results, as the classification results of this research shows. Each presented methodology has an overall accuracy and a Cohen's Kappa of above

0.90. The deep water class could be detected almost perfectly, while there was some misclassification of the shallow water class. Clouds are detected very well, but their shadows cause the largest misclassifications. With the application of open source machine learning and scientific data processing libraries, it becomes straightforward to efficiently experiment with different algorithms and parameters to determine the optimal classification routine for a certain application.

With improved classification of inland excess water inundations based on satellite imagery covering large areas, this research supports the operational defense against the floods, and helps to understand their development. The

inland excess water maps can be used as input for scientific study of the phenomenon and to support sustainable water management.

Acknowledgements

References

Abadi, M., Agarwal, A., Barham, P., Brevdo, E., Chen, Z., Citro, C., Corrado, G.S., Davis, A., Dean, J., Devin, M., Ghemawat, S., Goodfellow, I., Harp, A., Irving, G., Isard, M., Jozefowicz, R., Jia, Y., Kaiser, L., Kudlur, M., Levenberg, J., Mané, D., Schuster, M., Monga, R., Moore, S., Murray, D., Olah, C., Shlens, J., Steiner, B., Sutskever, I., Talwar, K., Tucker, P., Vanhoucke, V., Vasudevan,V., Viégas F., Vinyals, O., Warden, P., Wattenberg, M., Wicke, M., Yu, Y., Zheng, X. 2015. TensorFlow: Large-scale machine learning on heterogeneous systems. Software available from tensorflow.org.

Baamonde, S., Cabana, M., Sillero N., Penedo, M.G., Naveira, H., Novo, J. 2019. Fully automatic multi-temporal land cover classification using Sentinel-2 image data. *Procedia Computer Science 159*, 650–657. DOI: 10.1016/j.procs.2019.09.220

Balázs, B., Bíró, T., Dyke, G., Singh, S.K., Szabó, Sz. 2018. Extracting water-related features using reflectance data and principal component analysis of Landsat images. *Hydrological Sciences Journal 63*(2), 269–284. DOI: 10.1080/02626667.2018.1425802

Breiman, L. 2001. Random Forests. *Machine Learning* 45(5–32). DOI:10.1023/A:1010933404324

Büttner, G., 2012. Guidelines for verification and enhancement of high resolution layers produced under GMES initial operations (GIO) Land monitoring 2011–2013. EEA Report

Chatziantoniou, A., Petropoulos, G.P., Psomiadis E. 2017. Co-Orbital Sentinel 1 and 2 for LULC Mapping with Emphasis on Wetlands in a Mediterranean Setting Based on Machine Learning. *Remote Sensing* 9, 1259. DOI:10.3390/rs9121259

Chollet, F. 2015. Keras, https://keras.io [04-20-2020]

CLC, 2018. Corine Land Cover (CLC) 2018, Version 20. European Environment Agency. https://land.copernicus.eu/pan-european/corine-land-cover/clc2018 [04-20-2020]

Congalton, R.G., Green, K. 2008. Assessing the accuracy of remotely sensed data: principles and practices. CRC, Boca Raton London New York, 183 p

Csendes, B. Mucsi, L. 2016. Inland excess water mapping using hyperspectral imagery. *Geographica Pannonica* 20 (4), 191–196. DOI:10.18421/GP20.04-01

Drusch, M., Del Bello, U., Carlier, S., Colin, O., Fernandez, V., Gascon, F., Hoersch, B., Isola, C., Laberinti, P. Martimort, P., Meygret, A., Spoto, F., Sy, O., Marchese, F., Bargellini, P. 2012. Sentinel-2: ESA's Optical High-Resolution Mission for GMES Operational Services. *Remote Sensing of Environment* 120, 25–36, DOI: 10.1016/j.rse.2011.11.026

Feyisa, G.L., Meilby, H., Fensholt, R., Proud, S.R. 2014. Automated Water Extraction Index: A new technique for surface water mapping using Landsat imagery. *Remote Sensing of Environment* 140, 23–35

Foga, S., Scaramuzza, P.L., Guo, S., Zhu, Z., Dilley, R.D., Beckmann, T., Schmidt, G.L., Dwyer, D.J., Hughes, M.J., Laue, B. 2017. Cloud detection algorithm comparison and validation for operational Landsat data products. *Remote Sensing of Environment* 194, 379–390, DOI: 10.1016/j.rse.2017.03.026

Gudmann, A., Mucsi, L., Henits, L. 2019. A CORINE felszínborítási térkép automatikus előállításának lehetősége döntésifa-osztályozó segítségével. (Automatic land cover mapping using decision tree classifier). *Geodézia és Kartográfia* 71(2), 9–13. (in Hungarian)

Huang, C., Davis, L.S., Townshend, J.R.G. 2002. An assessment of support vector machines for land cover classification. *International Journal of Remote Sensing* 23(4), 725–749, DOI: 10.1080/01431160110040323

Jin, Y., Liu, X., Chen, Y., Liang, X. 2018. Land-cover mapping using Random Forest classification and incorporating NDVI time-series and texture: a case study of central Shandong. *International Journal of Remote Sensing* 39 (23), 8703–8723, DOI: 10.1080/01431161.2018.1490976

Lacaux, J.P., Tourre, Y.M., Vignolles, C., Ndione, J.A., Lafaye, M. 2007. Classification of ponds from high-spatial resolution remote sensing: Application to Rift Valley Fever epidemics in Senegal. *Remote Sensing of Environment* 106, 66–74. DOI: 10.1016/j.rse.2006.07.012

Mezősi G. 2017. Physical Geography of Hungary. Heidelberg, London, New York, Springer, 334 p

Ming, D., Zhou, T., Wang, M., Tan, T. 2016. Land cover classification using random forest with genetic algorithm-based parameter optimization. *J. Appl. Remote Sens.* 10 (3), 035021. DOI: 10.1117/1.jrs.10.035021

Mucsi, L., Henits, L. 2010. Creating excess water inundation maps by sub-pixel classification of medium resolution satellite images. *Journal of Environmental Geography* 3 (1–4), 31–40.

Paszke, A., Gross, S., Massa, F., Lerer, A., Bradbury, J., Chanan, G., Killeen, T., Lin, Z., Gimelshein, N., Antiga, L., Desmaison, A., Köpf, A., Yang, E., DeVito, Z., Raison, M., Tejani, A., Chilamkurthy, S., Steiner, B., Fang, L., Bai, J., Chintala, S. 2019. PyTorch: An imperative style high-performance deep learning library. *Proc. Adv. Neural Inf. Process. Syst.* 32, 8024–8035.

Pedregosa, F., Varoquaux, G., Gramfort, A., Michel, V., Thirion, B., Grisel, O.,Blondel, M., Prettenhofer, P., Weiss, R., Dubourg, V., Vanderplas, J., Passos, A., Cournapeau, D., Brucher, M., Perrot, M., Duchesnay, E. 2011. Scikit-learn: Machine Learning in Python. *Journal of Machine Learning Research* 12, 2825–2830

Rai, A.K., Mandal, N., Singh, A., Singh, K.K. 2020. Landsat 8 OLI Satellite Image Classification using Convolutional Neural Network. *Procedia Computer Science* 167, 987–993. DOI:10.1016/j.procs.2020.03.398

Rakonczai, J., Mucsi, L., Szatmári, J., Kovács, F., Csató, Sz. 2001. A belvizes területek elhatárolásának módszertani lehetőségei (Methods for delineation of inland excess water areas). A földrajz eredményei az új évezred küszöbén. Az I. Magyar Földrajzi Konferencia CD 14 p. (in Hungarian)

Shahtahmassebi, A., Yang, N., Wang, K., Moore, N., Shen, Z. 2013. Review of shadow detection and de-shadowing methods in remote sensing. *Chinese Geographical Science* 23, 403–420. DOI: 10.1007/s11769-013-0613-x

Shi D., Yang, X. 2015. Support Vector Machines for Land Cover Mapping from Remote Sensor Imagery. In: Li, J., Yang X. (eds.) Monitoring and Modeling of Global Changes: A Geomatics Perspective. Springer Remote Sensing/Photogrammetry, Dordrecht, DOI: 10.1007/978-94-017-9813-6_13

Szántó, G., Mucsi, L., van Leeuwen, B. 2008. Application of self-organizing neural networks for the delineation of excess water areas. *Journal of Env. Geogr.* 1 (3-4), 15–20.

Szantoi Z, Escobedo FJ, Abd-Elrahman A, Pearlstine L, Dewitt B, Smith S. 2015, Classifying spatially heterogeneous wetland communities using machine learning algorithms and spectral and textural features. *Environ Monit Assess* 187 (5), 262. DOI: 10.1007/s10661-015-4426-5

Szatmári, J., van Leeuwen, B. 2013. Inland Excess Water – Belvíz – Suvišne Unutrašnje Vode, Szeged, Újvidék, Szegedi Tudományegyetem, Újvidéki Egyetem, 154 p

Tanács E., Belényesi M., Lehoczki R., Pataki R., Petrik O., Standovár T., Pásztor L., Laborczi A., Szatmári G., Molnár Zs., Bede-Fazekas Á., Kisné Fodor L., Varga I., Zsembery Z., Maucha G. 2019. Országos, nagyfelbontású ökoszisztéma- alaptérkép: módszertan, validáció és felhasználási lehetőségek. (National high resolution ecosystem base map: Methodology, validation and possibilities for applications). *Természetvédelmi közlemények* 25, 34–58. DOI: 10.17779/tvk-jnatconserv.2019.25.34. (in Hungarian)

Thanh-Noi, P., Kappas, M. 2018. Comparison of Random Forest, k-Nearest Neighbor, and Support Vector Machine Classifiers for Land Cover Classification Using Sentinel-2 Imagery. *Sensors* 18 (2), 18. DOI: 10.3390/s18010018

van Leeuwen, B., Mezősi, G., Tobak, Z., Szatmári, J., Barta, K. 2012. Identification of inland excess water floodings using an artificial neural network. *Carpathian Journal of Earth and Environmental Sciences* 7 (4), 173–180.

van Leeuwen, B., Tobak, Z. 2014. Operational Identification of Inland Excess Water Floods Using Satellite Imagery, In: Vogler, R., Car, A., Strobl, J.Griesebner, G. (Eds.), GI_Forum 2014. Geospatial Innovation for Society. Herbert Wichmann Verlag, VDE Verlag GMBH, Berlin/Offenbach, 12–15. DOI: 10.1553/giscience2014s12

van Leeuwen, B., Tobak, Z., Kovács, F. 2020. Sentinel 1 and 2 based near real time inland excess water mapping for optimized water management. *Sustainability* 12 (7), 2854. DOI: 10.3390/su12072854

Zhu, X.X., Tuia, D., Mou, L., Xia, G-S.,Zhang, L., Xu, F., Fraundorfer, F. 2017. Deep Learning in Remote Sensing: A Comprehensive Review and List of Resources. *IEEE Geoscience and Remote Sensing Magazine* 5(4) 8–36. DOI: 10.1109/mgrs.2017.2762307